The Astrophysical Journal, 891:87 (8pp), 2020 March 1 https://doi.org/10.3847/1538-4357/ab722d

An Empirical "High-confidence" Candidate Zone for *Fermi* BL Lacertae Objects

Shi-Ju Kang[1,2], Kerui Zhu[3], Jianchao Feng[2,4], Qingwen Wu[5], Bin-Bin Zhang[6,7,8], Yue Yin[1], Fei-Fei Wang[9], Yu Liu[5], and Tian-Yuan Zheng[10]

[1] School of Physics and Electrical Engineering, Liupanshui Normal University, Liupanshui, Guizhou, 553004, People's Republic of China
kangshiju@alumni.hust.edu.cn
[2] Guizhou Provincial Key Laboratory of Radio Astronomy and Data Processing, Guiyang, Guizhou, 550001, People's Republic of China
[3] Department of Physics, Yunnan Normal University, Kunming, Yunnan, 650092, People's Republic of China
[4] School of Physics and Electronic Science, Guizhou Normal University, Guiyang, Guizhou, 550001, People's Republic of China
[5] School of Physics, Huazhong University of Science and Technology, Wuhan, Hubei, 430074, People's Republic of China
[6] School of Astronomy and Space Science, Nanjing University, Nanjing 210093, People's Republic of China
[7] Key Laboratory of Modern Astronomy and Astrophysics, Nanjing University, Ministry of Education, People's Republic of China
[8] Department of Physics and Astronomy, University of Nevada Las Vegas, NV 89154, USA
[9] School of Mathematics and Physics, Qingdao University of Science and Technology, Qingdao, Shandong, 266061, People's Republic of China
[10] The High School Affiliated to Anhui Normal University, Wuhu, Anhui, 241000, People's Republic of China
Received 2019 March 11; revised 2020 January 29; accepted 2020 January 30; published 2020 March 6

Abstract

In the third catalog of active galactic nuclei detected by the *Fermi* Large Area Telescope Clean (3LAC) sample, there are 402 blazar candidates of uncertain type (BCU). The proposed analysis will help to evaluate the potential optical classification flat spectrum radio quasars (FSRQs) versus BL Lacertae (BL Lac) objects of BCUs, which can help to understand which is the most elusive class of blazar hidden in the *Fermi* sample. By studying the 3LAC sample, we found some critical values of γ-ray photon spectral index ($\Gamma_{\rm ph}$), variability index (VI), and radio flux ($F_{\rm R}$) of the sources separate known FSRQs and BL Lac objects. We further utilize those values to defined an empirical "high-confidence" candidate zone that can be classified as BCUs. Within such a zone ($\Gamma_{\rm ph} < 2.187$, $\log F_{\rm R} < 2.258$, and $\log {\rm VI} < 1.702$), we found that 120 BCUs can be classified as BL Lac object candidates with a higher degree of confidence (with a misjudged rate <1%). Our results suggest that an empirical "high-confidence" diagnosis is possible to distinguish the BL Lac objects from the *Fermi* observations based on only the direct observational data of $\Gamma_{\rm ph}$, VI, and $F_{\rm R}$.

Unified Astronomy Thesaurus concepts: Blazars (164); BL Lacertae objects (158)

1. Introduction

Blazars are a particular class of radio-loud active galactic nuclei (AGNs) with a relativistic jet pointing toward the Earth. The broadband (from radio up to TeV energies) emissions of blazars are mainly dominated by nonthermal components that are produced in the relativistic jet (Urry & Padovani 1995). According to the strength of the optical spectral lines, blazars can be further divided into two subclasses (Stickel et al. 1991; Stocke et al. 1991; Laurent-Muehleisen et al. 1999), namely, the flat spectrum radio quasars (FSRQs; strong emission lines with equivalent width EW $\geqslant$ 5 Å in rest frame) and the BL Lacerate objects (BL Lac objects; weak or no emission and absorption lines). The multiwavelength spectral energy distributions (SEDs) from the radio to γ-ray bands normally exhibit a two-hump structure in the $\log\nu - \log\nu F_\nu$ space. The low energy bump (peaking between the millimeter and soft X-ray range) is always explained as synchrotron emission from the nonthermal electrons in the relativistic jet, while the high energy bump (peaking within MeV–GeV energy range) is inverse Compton scattering. Furthermore, based on the peak frequency ($\nu_{\rm p}^{\rm S}$) of the lower energy bump, blazars can also be classified as low- ($\nu_{\rm p}^{\rm S} < 10^{14}$ Hz), intermediate- (10^{14} Hz $< \nu_{\rm p}^{\rm S} < 10^{15}$ Hz), and high- ($\nu_{\rm p}^{\rm S} > 10^{15}$ Hz) synchrotron-peaked sources (i.e., LSPs, ISPs, and HSPs; Abdo et al. 2010).

This work utilizes the third catalog of AGNs detected by the *Fermi*-LAT (3LAC) sample (Ackermann et al. 2015), which is part of the first four years of the *Fermi*-LAT data, the third *Fermi* Large Area Telescope (LAT) source catalog (3FGL, Acero et al. 2015). The 3LAC clean sample (i.e., the high-confidence clean sample of the 3LAC) reports 1444 γ-ray AGNs: 414 FSRQs (~30%), 604 BL Lac objects (~40%), 402 blazar candidates of uncertain type (BCU, ~30%), and 24 nonblazar type AGNs (<2%) (Ackermann et al. 2015). The identification of FSRQs and BL Lac objects are solid, mostly based on the clear evidence of the (non)existing emission and/or absorption lines. On the other hand, BCUs are sources without a confirmed classification due to the missing representative features on optical spectrum (BCU I), synchrotron peak frequencies of SED (BCU II), and/or their broadband emissions (BCU III) (see Acero et al. 2015; Ackermann et al. 2015 for the details and references therein). Studying such a large sample of BCUs is crucial to understand of the physics of γ-ray emission of blazars (e.g., Singal et al. 2012; Singal 2015; Fan et al. 2016; Kang et al. 2018, 2019a, 2019b; Zhu et al. 2020).

Estimating the possible classification BL Lac object versus FSRQ of BCUs can help to understand which is the most elusive class of blazar hidden in the *Fermi* sample (Massaro et al. 2015). Indeed, some potential BL Lac object or FSRQ candidates can be identified from the BCU sample in the 2FGL/3FGL catalogs using different approaches such as supervised machine learning (e.g., support vector machine [SVM] and random forest [RF]; Hassan et al. 2013), neural

network (Chiaro et al. 2016), artificial neural network (ANN; Salvetti et al. 2017), multivariate classification method (Lefaucheur & Pita 2017), and statistical analysis of the broadband spectral properties (including spectral indices in the gamma-ray, X-ray, optical, and radio bands; Yi et al. 2017). In addition, we have identified potential BL Lac object and FSRQ candidates from the 3LAC Clean sample using four different SML algorithms (Mclust Gaussian finite mixture models, Decision trees, RF, and SVM; Kang et al. 2019a, Paper I) and from the 4FGL catalog using three different SML algorithms (ANN, RF, and SVM; Kang et al. 2019b). Nevertheless, the final confirmation of the BCU nature of candidates in all above approaches is subject to the observations of optical spectroscopy or counterparts in other wavelengths (e.g., Massaro et al. 2014, 2016; Marchesini et al. 2016; Marchesi et al. 2018; Marchesini et al. 2019; Álvarez Crespo et al. 2016a, 2016b, 2016c; Klindt et al. 2017; Peña-Herazo et al. 2017, 2019; Desai et al. 2019), or broadband spectral features (e.g., Fermi/LAT collaboration, Álvarez Crespo et al. 2016a, 2016b, 2016c; Massaro et al. 2009, 2012, 2016). If such information is missing, classification of BCUs will become challenging especially when no training set is available (see, e.g., Shaw et al. 2013; Landoni et al. 2015, 2018; Ricci et al. 2015; Paiano et al. 2017a, 2017b; Kaur et al. 2019). To overcome such difficulties, in this study, we aim to evaluate the potential classification of BCUs based on only the direct observational properties in γ-ray and radio bands. Such properties include γ-ray photon spectral index ($\Gamma_{\rm ph}$), variability index (VI), and radio flux ($F_{\rm R}$). By performing a detailed analysis, we confirmed the existence of a high-confident zone where the condition-met BCUs are most likely BL Lac objects.

We organize the present paper as follows. In Section 2, a brief description of the sample selection is provided followed by the proposed analysis methods and results. Comparisons of our results with other recent results are presented in Section 3. Our results are discussed in Section 4 and summarized in Section 5.

2. Data Selection and Analysis

We selected the data from the 3LAC Clean sample[11] in the 3FGL Catalog.[12] In order to perform the analysis, we selected the sources with available measurements of $\Gamma_{\rm ph}$, VI, and $F_{\rm R}$, which yielded a sample of 1418 Fermi blazars, including 414 FSRQs, 604 BL Lac objects, and 400 BCUs (two sources that have no radio data are excluded).

In order to investigate whether there is a characteristic zone in the three parameters (namely, $\Gamma_{\rm ph}$, VI, and $F_{\rm R}$), we first exhibited the scatterplots of the known FSRQ and BL Lac object samples. In Figure 1, the 2D scatterplots between any two parameters of $\Gamma_{\rm ph}$, VI, and $F_{\rm R}$ for the identified FSRQs and BL Lac objects are shown in the left column. One can immediately notice that the values of $\Gamma_{\rm ph}$, VI, and $F_{\rm R}$ of the FSRQs are normally larger than those of the BL Lac objects. FSRQs feature a comparatively concentrated distribution, while the BL Lac objects show a relatively wider distribution. The distributions of $\Gamma_{\rm ph}$, VI, and $F_{\rm R}$ between the FSRQ and BL Lac object groups exhibit significantly different behavior. The two-sample Kolmogorov–Smirnov test for these three parameters gives the value of the test statistic $D = 0.514$ and the p-value $p_1 = 0$; the Welch Two Sample t-test gives the value of the t-statistic $t = 32$, the degrees of freedom for the t-statistic $df = 2455$, and the p-value $p_2 < 1.0\text{E}{-6}$; while the Wilcoxon rank sum test with the continuity correction gives the value of the test statistic $W = 1826{,}100$ and p-value $p_3 < 1.0\text{E}{-6}$ (obtained by R[13] code R Core Team 2019) for all three parameters (see Table 1). For the other parameter combinations, either one or two parameters, the test results are also listed in Table 1. The results significantly reject the hypothesis that the two distributions (FRSQs, BL Lac objects) are drawn from the same distribution.

We find that the two samples (marked red and blue) can be well separated by some critical lines with the following values: $\Gamma_{\rm ph} = 2.187$, $\log F_{\rm R} = 2.258$, and $\log {\rm VI} = 1.702$. The three critical values are obtained through the following procedure:

1. We performed a one-sample normal distribution test (e.g., KS-test, t-test, and Wilcoxon-test) for the $\Gamma_{\rm ph}$, VI, and $F_{\rm R}$ of the FSRQs and found that the distribution of those parameters are consistent with a Gaussian distribution with a significant p-value (Table 2).
2. We further obtained the lowest one-sided confidence interval value ($a_1 = 2.187$, $a_2 = 2.258$, and $a_3 = 1.702$) under the assumptions that $\Gamma_{\rm ph}$, VI, and $F_{\rm R}$ of FSRQs are normally distributed, which are assigned as the critical value mentioned above.

We find that there are no FSRQs falling in the range $\Gamma_{\rm ph} < a_1$, $\log F_{\rm R} < a_2$ and $\log {\rm VI} < a_3$, while some BL Lac objects lie in the zone ($a_i < X$), where a_i ($i = 1, 2, 3$) is set as the boundary value. Moreover, there are only three FSRQs in the range of $a_i < X$ ($\Gamma_{\rm ph} = 2.187$, $\log F_{\rm R} = 2.258$, and $\log {\rm VI} = 1.702$), where the misjudged rate $\eta = 3/414 \simeq 0.725\%$ for FSRQs is obtained. Here the misjudged rate η is a probability that an FSRQ is misclassified as a BL Lac object, which is defined as $\eta = N_{err}/N_F$, where N_F is the total number of FSRQs and $N_{\rm err}$ is the number of FSRQs that are misclassified as BL Lac objects at the $a_i < X$ range.

In order to test our hypothesis, we randomly divide FSRQs into 10 subsamples with one subsample reserved as the verification data, and the remaining nine subsamples used as the training data. Then, the proposed analysis is repeated 10 times (the 10 folds), the misjudged rate η is repeatedly calculated 10 times. Finally, by averaging the 10 misjudged rates, a 10-fold cross-validation[14] misjudged rate $\eta = 0.971\%$ is obtained for the FSRQs. This result suggests that the zone of $a_i < X$ (e.g., the lowest one-sided confidence interval value for a 1σ confidence level with $\simeq$0.725% false positive rate for FSRQs) can be treated as an "inviable" region for the FSRQs or as a candidate zone for the BL Lac objects, called "$a_i < X$ candidate zone" for BL Lac objects.

Finally, we can test the "$a_i < X$ candidate zone" in the BCU sample. We obtain 120 BL Lac object candidates which fall into the high-confidence zone with the following three conditions satisfied: $\Gamma_{\rm ph} < 2.187$, $\log F_{\rm R} < 2.258$, and $\log$

[11] http://www.asdc.asi.it/fermi3lac/
[12] https://fermi.gsfc.nasa.gov/ssc/data/access/lat/4yr_catalog/
[13] https://www.r-project.org/
[14] In a K-fold cross-validation, the original samples are randomly divided into K subsamples. Among the K subsamples, one subsample is reserved as the verification data of the test model, and the remaining K-1 subsamples are used as the training data. Then, the cross-validation process is repeated K times (multiple times), and each of the K subsamples is accurately used as the verification data. The K results resulting from the folding can then be averaged (or otherwise combined) to produce a single estimate.

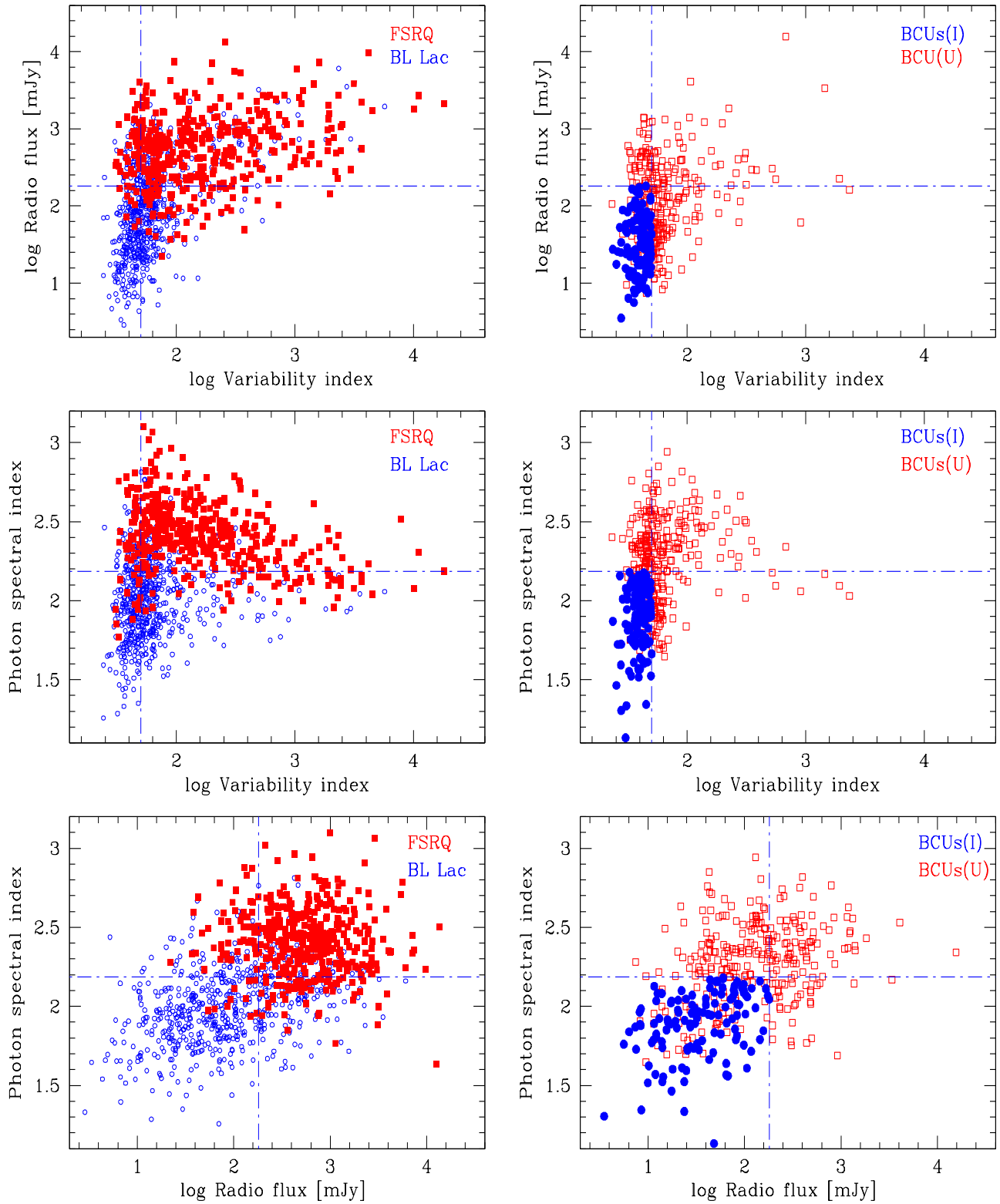

Figure 1. Scatterplots of the VI, F_R, and Γ_{ph} for *Fermi* blazars (left column), where red solid squares represent FSRQs and blue empty points represent BL Lac objects. The right panels represent the scatterplots of the BCUs (right column), where the BCUs (I) are the identified BL Lacs (blue solid points) using the "$a_i < X$ zone" and the BCUs (U) are the unidentified BCUs (red empty squares). The dotted–dashed parallel and perpendicular blue lines indicate that Γ_{ph}, log F_R, and log VI are equal to 2.187, 2.258, and 1.702, respectively.

VI < 1.702. These 120 sources are plotted as blue solid circles in Figure 1 (right column) and listed in Table 3, while the red empty squares mark the rest of the unidentified optical classification BCUs.

3. Comparison with Literature Results

We then compared our 120 identified BL Lac object candidates with some other recent studies. We found that our

Table 1
The Result of the Two-sample Test

Test Data Set	Using Parameters	KS-test		t-test			Wilcoxon-test	
		D	p_1	t	df	p_2	W	p_3
604 BL Lac objects versus 414 FSRQs	Γ_{ph}, log VI, log F_R	0.514	0	32	2455	<1.0E−6	1826100	<1.0E−6
	Γ_{ph}, log F_R	0.587	0	31	1915	<1.0E−6	850970	<1.0E−6
	Γ_{ph}, log VI	0.497	0	25	1399	<1.0E−6	803250	<1.0E−6
	log VI, log F_R	0.490	0	25	1596	<1.0E−6	802600	<1.0E−6
	Γ_{ph}	0.627	0	27	955	<1.0E−6	222270	<1.0E−6
	log F_R	0.562	0	23	996	<1.0E−6	210750	<1.0E−6
	log VI	0.478	0	15	608	<1.0E−6	197720	<1.0E−6
120 BL Lac objects versus 414 FSRQs	Γ_{ph}, log VI, log F_R	0.725	0	38	926	<1.0E−6	416470	<1.0E−6
	Γ_{ph}, log F_R	0.849	0	32	427	<1.0E−6	192930	<1.0E−6
	Γ_{ph}, log VI	0.659	0	29	770	<1.0E−6	179540	<1.0E−6
	log VI, log F_R	0.753	0	35	803	<1.0E−6	188340	<1.0E−6
	Γ_{ph}	0.848	0	24	198	<1.0E−6	48137	<1.0E−6
	log F_R	0.862	0	28	231	<1.0E−6	48580	<1.0E−6
	log VI	0.884	0	24	461	<1.0E−6	47636	<1.0E−6

Note. Column 1 shows the test data set: 604 BL Lac objects versus 414 FSRQs, or 120 BL Lac object candidates versus 414 FSRQs. Column 2 shows the parameters satisfied simultaneously used in the test. Columns 3 and 4 give the value of the test statistic (D) and the p-value (p_1) for the two-sample Kolmogorov–Smirnov test; the value of the t-statistic (t), the degrees of freedom for the t-statistic (df) and the p-value (p_2) for the Welch Two Sample t-test are listed in Column 5, Column 6, and Column 7, respectively; Column 8 and Column 9 report the value of the test statistic (W) and the p-value (p_3) for the Wilcoxon rank sum test with a continuity correction. All data are obtained by the R code (https://www.r-project.org/) (see R Core Team 2019).

Table 2
The Result of the One-sample Test

Test Data Set	Using Parameter	KS-test		t-test			Wilcoxon-test	
		D	p_1	t	df	p_2	W	p_3
414 FSRQs	Γ_{ph}	0.964	0	226	413	0	85905	<1.0E−6
	logF_R	0.942	0	118	413	<1.0E−6	85905	<1.0E−6
	log VI	0.931	0	85	413	<1.0E−6	85905	<1.0E−6

Note. Column 1 shows the test data set: the three parameters of the 414 FSRQs. Column 2 shows the parameter used in the one-sample test. Column 3 and Column 4 give the value of the test statistic (D) and the p-value (p_1) for the One-sample Kolmogorov–Smirnov test. The value of the t-statistic (t), the degrees of freedom for the t-statistic (df), and the p-value (p_2) for the Welch One Sample t-test are listed in Column 5, Column 6, and Column 7, respectively; Column 8 and Column 9 report the value of the test statistic (W) and the p-value (p_3) for the Wilcoxon signed rank test with a continuity correction. All data are obtained by the R code (https://www.r-project.org/) (see R Core Team 2019.)

results are mostly consistent with previous works presented in Chiaro et al. (2016), Lefaucheur & Pita (2017), Yi et al. (2017), and Kang et al. (2019a) which utilize different statistical (e.g., SML) algorithms (see Tables 4 and 3). The exceptions are as follows: two sources did not find matching sources and two sources did not provide a clear classification in Lefaucheur & Pita (2017). In addition, only three sources are classified as FSRQs in Mclust Gaussian Mixture Modeling (M_8), and two are classified as FRSQs using SVM (SVM_8) using eight parameters in Kang et al. (2019a); one source is classified as an FSRQ in Chiaro et al. (2016, Chi16), whereas two sources are classified as FRSQs in Yi et al. (2017) (Y17). The results, provided in Table 4, indicate that the highest mismatch rate (e.g., rate $= 3/120\% \sim 2.5\%$) is less than 3%. Hence, the selected area ($a_i < X$ candidate zone) shows a higher degree of confidence.

For these 120 identified BL Lac object candidates in the work, of which 41 sources are identified as BL Lac object-type in the 3FHL catalog (Ajello et al. 2017, 3FHL, see Table 4); and 63 sources are identified as BL Lac object-type in the 4FGL catalog (see 4FGL FITS table "gll_psc_v20.fit"[15] of The Fermi-LAT collaboration 2019, 4FGL). Only one source is classified as an FSRQ in the 4FGL catalog (The Fermi-LAT collaboration 2019). There are 24, 2, 11, 10, 12, and 15 sources that have been identified as the BL Lac object-type by Massaro et al. (2016, M16), Desai et al. (2019, D19), Marchesini et al. (2019, M19), Marchesi et al. (2018, M18), Peña-Herazo et al. (2017, P17), and Álvarez Crespo et al. (2016b, A16) using spectroscopic observations, respectively. After cross-matching these results (3FHL, M16, D19, M19, M18, P17, A16, and 4FGL), 74 sources are obtained (also see Tables 4 and 3). Here, the remaining ones ("46 sources") need to be further tested and confirmed by spectroscopic observations.

4. Discussions

As shown in Paper I or other similar works, the SML method can return the probabilities P_{Bi} and P_{Fi} (e.g., see the machine-readable supplementary material in Table 4 in Kang et al. 2019a) that a BCU i belongs to the BL Lac objects (B) or FSRQs (F) classes, respectively. These probabilities can help to distinguish each source belonging to each class. However, it should be noted that SML algorithms provide a statistical approach (or other statistical algorithms) to address the

[15] https://fermi.gsfc.nasa.gov/ssc/data/access/lat/8yr_catalog/gll_psc_v20.fit

Table 3
The Identified BL Lac Object Candidates Using the "$a_i < X$ Candidate Zone"

3FGL name (1)	Class (2)	SED (3)	$\log F_R$ (4)	Γ_{ph} (5)	log VI (6)	X (7)	M_8 (8)	DT_8 (9)	RF_8 (10)	SVM_8 (11)	LP17 (12)	Chi16 (13)	Y17 (14)	$Class_O$ (15)
3FGL J0003.2−5246	BCU	HSP	1.681	1.815	1.895	bll	bll	bll	bll	bll	bll	bll	bll	⋯
3FGL J0017.2−0643	BCU	LSP	1.573	1.973	2.116	bll	bll	bll	bll	bll	bll	bll	bll	⋯
3FGL J0031.3+0724	BCU	HSP	1.519	1.086	1.824	bll	bll	bll	bll	bll	bll	bll	bll	bll (e, h)
3FGL J0039.0−2218	BCU	HSP	1.563	2.069	1.715	bll	bll	bll	bll	bll	bll	bll	bll	⋯
3FGL J0039.1+4330	BCU	⋯	1.549	0.913	1.963	bll	bll	bll	bll	bll	bll	bll	bll	⋯
3FGL J0040.3+4049	BCU	⋯	1.481	1.683	1.132	bll	bll	bll	bll	bll	bll	bll	bll	bll(e, h)
3FGL J0040.5−2339	BCU	ISP	1.692	1.730	1.946	bll	bll	bll	bll	bll	bll	bll	bll	bll(g, h)
3FGL J0043.5−0444	BCU	HSP	1.605	1.475	1.735	bll	bll	bll	bll	bll	bll	bll	bll	bll(a, b, c, h)
3FGL J0043.7−1117	BCU	HSP	1.442	1.397	1.594	bll	bll	bll	bll	bll	bll	bll	bll	bll (h)
3FGL J0051.2−6241	BCU	HSP	1.701	1.635	1.663	bll	bll	bll	bll	bll	bll	bll	bll	bll(c, h)
3FGL J0107.0−1208	BCU	ISP	1.514	1.778	2.180	bll	bll	bll	bll	bll	bll	bll	bll	⋯
3FGL J0116.2−2744	BCU	⋯	1.606	1.237	2.023	bll	bll	bll	bll	bll	bll	bll	bll	bll (h)
3FGL J0121.7+5154	BCU	⋯	1.586	0.928	1.984	bll	bll	bll	bll	bll	bll	bll	bll	⋯
3FGL J0127.2+0325	BCU	HSP	1.695	1.208	1.899	bll	bll	bll	bll	bll	bll	bll	bll	bll(c, d, e, h)
3FGL J0139.9+8735	BCU	ISP	1.624	1.063	1.891	bll	bll	bll	bll	bll	bll	bll	bll	⋯
3FGL J0150.5−5447	BCU	HSP	1.643	1.641	2.118	bll	bll	bll	bll	bll	bll	bll	bll	⋯
3FGL J0156.9−4742	BCU	HSP	1.494	1.458	2.009	bll	bll	bll	bll	bll	bll	bll	bll	bll(a, b, c, h)
3FGL J0211.2−0649	BCU	ISP	1.520	1.347	2.100	bll	bll	bll	bll	bll	bll	bll	bll	bll (g)
3FGL J0213.1−2720	BCU	LSP	1.548	1.690	2.089	bll	bll	bll	bll	bll	bll	bll	bll	⋯
3FGL J0228.7−3106	BCU	ISP	1.541	1.992	2.140	bll	bll	bll	bll	bll	bll	bll	fsrq	⋯
3FGL J0232.9+2606	BCU	ISP	1.530	1.993	2.086	bll	bll	bll	bll	bll	bll	bll	bll	bll(c, h)
3FGL J0255.8+0532	BCU	LSP	1.602	2.017	2.070	bll	bll	bll	bll	bll	bll	bll	bll	bll(a, b, h)
3FGL J0301.8−2721	BCU	LSP	1.432	1.722	2.158	bll	bll	bll	bll	bll	bll	bll	bll	⋯
3FGL J0342.6−3006	BCU	LSP	1.567	2.195	1.846	bll	bll	bll	bll	bll	bll	bll	bll	⋯
3FGL J0431.6+7403	BCU	HSP	1.612	1.485	1.988	bll	bll	bll	bll	bll	bll	bll	bll	bll(e, h)
3FGL J0434.6+0921	BCU	ISP	1.691	2.074	2.115	bll	bll	bll	bll	bll	bll	bll	bll	bll(e, h)
3FGL J0439.6−3159	BCU	HSP	1.562	1.039	1.771	bll	bll	bll	bll	bll	bll	bll	bll	⋯
3FGL J0506.9−5435	BCU	HSP	1.635	1.255	1.603	bll	bll	bll	bll	bll	bll	bll	bll	bll(c, h)
3FGL J0515.5−0123	BCU	⋯	1.523	1.994	1.755	bll	fsrq	bll	bll	bll	bll	bll	bll	⋯
3FGL J0602.8−4016	BCU	HSP	1.696	1.873	1.923	bll	bll	bll	bll	bll	bll	bll	bll	bll(c, h)
3FGL J0611.2+4323	BCU	HSP	1.633	1.644	2.168	bll	bll	bll	bll	bll	bll	bll	bll	⋯
3FGL J0626.6−4259	BCU	⋯	1.684	1.149	1.740	bll	bll	bll	bll	bll	bll	bll	bll	bll(c, d, h)
3FGL J0649.6−3138	BCU	HSP	1.668	0.877	1.729	bll	bll	bll	bll	bll	bll	bll	bll	bll(c, d, h)
3FGL J0652.0−4808	BCU	HSP	1.580	1.856	2.044	bll	bll	bll	bll	bll	bll	bll	bll	⋯
3FGL J0730.5−6606	BCU	HSP	1.614	1.910	1.789	bll	bll	bll	bll	bll	bll	bll	bll	bll(a, b, c, h)
3FGL J0742.4−8133c	BCU	⋯	1.404	1.246	1.464	bll	bll	bll	bll	bll	⋯	bll	bll	⋯
3FGL J0746.9+8511	BCU	HSP	1.571	1.057	1.787	bll	bll	bll	bll	bll	bll	bll	bll	⋯
3FGL J0827.2−0711	BCU	HSP	1.597	2.241	2.067	bll	bll	bll	bll	bll	bll	bll	bll	bll(a, b, c, d, h)
3FGL J0917.3−0344	BCU	HSP	1.652	1.508	1.764	bll	bll	bll	bll	bll	bll	bll	bll	bll(h)
3FGL J0921.0−2258	BCU	HSP	1.510	1.158	1.553	bll	bll	bll	bll	bll	bll	bll	bll	bll(a, b, c, h)
3FGL J0947.1−2542	BCU	HSP	1.684	1.624	1.950	bll	bll	bll	bll	bll	bll	bll	bll	bll(c, d, h)
3FGL J0953.1−7657c	BCU	ISP	1.567	1.378	1.912	bll	bll	bll	bll	bll	⋯	bll	bll	⋯
3FGL J1040.8+1342	BCU	HSP	1.552	0.748	1.760	bll	bll	bll	bll	bll	bll	bll	bll	bll(a, b, c, h)
3FGL J1042.0−0557	BCU	HSP	1.618	1.923	1.944	bll	bll	bll	bll	bll	bll	bll	bll	bll (h)
3FGL J1042.1−4126	BCU	HSP	1.649	1.310	1.976	bll	bll	bll	bll	bll	bll	bll	bll	⋯
3FGL J1052.8−3741	BCU	ISP	1.549	1.803	1.996	bll	bll	bll	bll	bll	bll	bll	bll	bll(c, g, h)
3FGL J1125.0−2101	BCU	HSP	1.627	1.561	1.784	bll	bll	bll	bll	bll	bll	bll	bll	bll(a, b, c, d, h)
3FGL J1141.2+6805	BCU	HSP	1.666	1.353	1.611	bll	bll	bll	bll	bll	bll	bll	bll	⋯
3FGL J1141.6−1406	BCU	HSP	1.634	1.777	2.176	bll	bll	bll	bll	bll	bll	bll	bll	bll(b, h)
3FGL J1153.7−2555	BCU	⋯	1.603	1.927	2.015	bll	bll	bll	bll	bll	bll	bll	bll	⋯
3FGL J1155.4−3417	BCU	HSP	1.488	1.377	1.335	bll	bll	bll	bll	bll	bll	bll	bll	bll (f)
3FGL J1156.7−2250	BCU	HSP	1.584	1.235	1.890	bll	bll	bll	bll	bll	bll	bll	bll	⋯
3FGL J1158.9+0818	BCU	⋯	1.559	0.869	1.870	bll	bll	bll	bll	bll	bll	bll	bll	⋯
3FGL J1159.6−0723	BCU	LSP	1.654	1.887	2.104	bll	bll	bll	bll	bll	bll	bll	bll	bll(c, h)
3FGL J1203.5−3925	BCU	HSP	1.602	1.811	1.639	bll	bll	bll	bll	bll	bll	bll	bll	bll(c, d, h)
3FGL J1207.6−4537	BCU	⋯	1.535	2.221	2.113	bll	fsrq	bll	bll	fsrq	bll	bll	bll	⋯
3FGL J1223.3−3028	BCU	HSP	1.581	0.918	1.887	bll	bll	bll	bll	bll	bll	bll	bll	bll (f)
3FGL J1258.7+5137	BCU	⋯	1.611	1.705	2.159	bll	bll	bll	bll	bll	bll	bll	bll	⋯
3FGL J1314.7−4237	BCU	HSP	1.653	1.143	2.082	bll	bll	bll	bll	bll	bll	bll	bll	bll (h)
3FGL J1315.4+1130	BCU	HSP	1.692	1.316	1.962	bll	bll	bll	bll	bll	unc	bll	bll	bll(a, b, c, h)
3FGL J1342.7+0945	BCU	ISP	1.373	1.439	1.870	bll	bll	bll	bll	bll	bll	bll	bll	fsrq
3FGL J1346.9−2958	BCU	ISP	1.662	1.439	1.744	bll	bll	bll	bll	bll	bll	bll	bll	bll(b, c, h)
3FGL J1356.3−4029	BCU	ISP	1.648	1.881	2.060	bll	bll	bll	bll	bll	bll	bll	bll	⋯
3FGL J1406.0−2508	BCU	HSP	1.660	1.489	1.893	bll	bll	bll	bll	bll	bll	bll	bll	bll(b, c, h)
3FGL J1427.8−3215	BCU	ISP	1.557	1.086	2.036	bll	bll	bll	bll	bll	bll	bll	bll	bll(c, h)
3FGL J1434.6+6640	BCU	HSP	1.592	0.997	1.517	bll	bll	bll	bll	bll	bll	bll	bll	bll(b, c, h)
3FGL J1440.0−3955	BCU	HSP	1.610	1.300	1.864	bll	bll	bll	bll	bll	bll	bll	bll	bll (g)
3FGL J1446.8−1831	BCU	HSP	1.415	1.409	1.723	bll	bll	bll	bll	bll	bll	bll	bll	⋯
3FGL J1507.6−3710	BCU	ISP	1.611	1.898	2.131	bll	bll	bll	bll	bll	bll	bll	bll	⋯
3FGL J1511.8−0513	BCU	⋯	1.677	1.244	2.034	bll	bll	bll	bll	bll	bll	bll	bll	bll(b, c, h)

Table 3
(Continued)

3FGL name (1)	Class (2)	SED (3)	$\log F_R$ (4)	Γ_{ph} (5)	log VI (6)	X (7)	M_8 (8)	DT_8 (9)	RF_8 (10)	SVM_8 (11)	LP17 (12)	Chi16 (13)	Y17 (14)	$Class_O$ (15)
3FGL J1512.2−2255	BCU	HSP	1.611	1.285	1.907	bll	bll	bll	bll	bll	bll	bll	bll	bll(c, d, h)
3FGL J1539.8−1128	BCU	HSP	1.612	1.897	2.085	bll	bll	bll	bll	bll	bll	bll	bll	bll(c, d, h)
3FGL J1547.1−2801	BCU	HSP	1.628	1.677	1.708	bll	bll	bll	bll	bll	bll	bll	bll	bll(c, d, h)
3FGL J1549.7−0658	BCU	HSP	1.689	1.117	1.924	bll	bll	bll	bll	bll	bll	bll	bll	⋯
3FGL J1559.8−2525	BCU	⋯	1.493	1.657	1.944	bll	bll	bll	bll	bll	bll	bll	bll	bll (g)
3FGL J1626.4−7640	BCU	ISP	1.692	2.113	1.990	bll	bll	bll	bll	bll	bll	bll	bll	bll(b, c, h)
3FGL J1636.7+2624	BCU	ISP	1.571	1.312	2.039	bll	bll	bll	bll	bll	bll	bll	bll	bll(a, b, h)
3FGL J1643.6−0642	BCU	HSP	1.694	1.459	2.071	bll	bll	bll	bll	bll	bll	bll	bll	bll (h)
3FGL J1656.8−2010	BCU	HSP	1.680	1.572	1.961	bll	bll	bll	bll	bll	bll	bll	bll	bll(a, b, c, d, h)
3FGL J1711.6+8846	BCU	⋯	1.587	1.077	1.570	bll	bll	bll	bll	bll	bll	bll	bll	⋯
3FGL J1714.1−2029	BCU	HSP	1.655	0.931	1.344	bll	bll	bll	bll	bll	bll	bll	bll	⋯
3FGL J1716.7−8112	BCU	HSP	1.623	2.028	2.060	bll	bll	bll	bll	bll	bll	bll	bll	bll (h)
3FGL J1719.3+1206	BCU	ISP	1.483	1.760	2.078	bll	bll	bll	bll	bll	bll	bll	bll	⋯
3FGL J1735.4−1118	BCU	LSP	1.659	1.926	2.156	bll	bll	bll	bll	bll	bll	fsrq	bll	⋯
3FGL J1740.4+5347	BCU	LSP	1.616	1.693	2.019	bll	bll	bll	bll	bll	bll	bll	bll	bll(c, h)
3FGL J1757.1+1533	BCU	LSP	1.653	2.256	2.045	bll	bll	bll	bll	fsrq	bll	bll	bll	⋯
3FGL J1820.3+3625	BCU	HSP	1.546	1.143	1.777	bll	bll	bll	bll	bll	bll	bll	bll	bll(e, h)
3FGL J1824.4+4310	BCU	ISP	1.443	1.528	1.725	bll	bll	bll	bll	bll	bll	bll	bll	⋯
3FGL J1838.5−6006	BCU	HSP	1.639	1.901	1.857	bll	bll	bll	bll	bll	bll	bll	bll	⋯
3FGL J1841.2+2910	BCU	HSP	1.604	1.811	1.567	bll	bll	bll	bll	bll	bll	bll	bll	bll(e, h)
3FGL J1848.1−4230	BCU	⋯	1.598	2.009	1.951	bll	bll	bll	bll	bll	bll	bll	bll	⋯
3FGL J1855.1−6008	BCU	⋯	1.499	1.922	1.813	bll	bll	bll	bll	bll	bll	bll	bll	bll(c, h)
3FGL J1904.5+3627	BCU	HSP	1.583	1.995	2.098	bll	bll	bll	bll	bll	bll	bll	bll	bll(e, h)
3FGL J1913.9+4441	BCU	HSP	1.481	1.192	1.851	bll	bll	bll	bll	bll	bll	bll	bll	bll(b, c, h)
3FGL J1939.6−4925	BCU	–	1.621	1.009	1.624	bll	bll	bll	bll	bll	bll	bll	bll	–
3FGL J1944.1−4523	BCU	HSP	1.591	1.828	1.560	bll	bll	bll	bll	bll	bll	bll	bll	⋯
3FGL J1954.9−5640	BCU	HSP	1.644	0.924	1.878	bll	bll	bll	bll	bll	bll	bll	bll	bll (g)
3FGL J1955.0−1605	BCU	HSP	1.494	1.394	2.047	bll	bll	bll	bll	bll	bll	bll	bll	bll(a, b, c, d, h)
3FGL J1955.9+0212	BCU	⋯	1.607	1.507	1.927	bll	bll	bll	bll	bll	bll	bll	bll	bll(c, h)
3FGL J1959.8−4725	BCU	HSP	1.695	1.377	1.524	bll	bll	bll	bll	bll	bll	bll	bll	bll(c, h)
3FGL J2002.7+6303	BCU	LSP	1.634	1.065	2.127	bll	bll	bll	bll	bll	bll	bll	bll	⋯
3FGL J2014.5+0648	BCU	HSP	1.650	1.203	1.915	bll	bll	bll	bll	bll	bll	bll	bll	bll(c, h)
3FGL J2017.6−4110	BCU	HSP	1.590	2.159	2.160	bll	bll	bll	bll	bll	bll	bll	fsrq	⋯
3FGL J2026.3+7644	BCU	HSP	1.505	0.805	1.839	bll	bll	bll	bll	bll	bll	bll	bll	⋯
3FGL J2031.0+1937	BCU	HSP	1.671	1.754	1.826	bll	bll	bll	bll	bll	bll	bll	bll	bll(b, c, h)
3FGL J2036.6−3325	BCU	HSP	1.443	0.547	1.305	bll	bll	bll	bll	bll	unc	bll	bll	bll(b, c, h)
3FGL J2046.7−1011	BCU	HSP	1.550	2.026	1.609	bll	bll	bll	bll	bll	bll	bll	bll	bll (g)
3FGL J2104.2−0211	BCU	HSP	1.528	1.150	1.524	bll	bll	bll	bll	bll	bll	bll	bll	bll(a, b, c, h)
3FGL J2133.3+2533	BCU	ISP	1.608	1.600	2.010	bll	bll	bll	bll	bll	bll	bll	bll	bll (h)
3FGL J2212.6+2801	BCU	LSP	1.600	2.161	1.791	bll	bll	bll	bll	bll	bll	bll	bll	bll(e, g, h)
3FGL J2213.6−4755	BCU	⋯	1.562	1.436	1.889	bll	bll	bll	bll	bll	bll	bll	bll	bll (g)
3FGL J2220.3+2812	BCU	HSP	1.579	1.689	1.833	bll	bll	bll	bll	bll	bll	bll	bll	bll(e, h)
3FGL J2232.9−2021	BCU	HSP	1.511	1.099	2.081	bll	bll	bll	bll	bll	bll	bll	bll	bll(a, b, h)
3FGL J2243.2−3933	BCU	LSP	1.530	1.773	2.119	bll	bll	bll	bll	bll	bll	bll	bll	⋯
3FGL J2251.5−4928	BCU	ISP	1.689	1.522	1.967	bll	bll	bll	bll	bll	bll	bll	bll	bll(c, h)
3FGL J2305.3−4219	BCU	LSP	1.614	1.600	2.048	bll	bll	bll	bll	bll	bll	bll	bll	bll (g)
3FGL J2312.9−6923	BCU	⋯	1.581	1.086	1.804	bll	bll	bll	bll	bll	bll	bll	bll	⋯
3FGL J2316.8−5209	BCU	ISP	1.543	1.408	1.735	bll	bll	bll	bll	bll	bll	bll	bll	bll (g)
3FGL J2322.9−4917	BCU	HSP	1.634	1.452	1.957	bll	bll	bll	bll	bll	bll	bll	bll	bll(c, h)
3FGL J2353.3−4805	BCU	⋯	1.457	1.947	2.011	bll	fsrq	bll	bll	bll	bll	bll	bll	⋯

Note. Column 1 shows the 3FGL names. Column 2 lists the optical class (BCU reported in Acero et al. 2015). Column 3 gives the SED classifications (LSP, ISP, and HSP); the radio flux (log F_R) is listed in Column 4. The γ-ray photon spectral index (Γ_{ph}) and γ-ray variability index (log VI) are shown in Columns 5 and 6, respectively. The BL Lac object candidates using the "$a_i < X$ candidate zone" are listed in Column 7. Columns 8–11 (M_8, DT_8, RF_8, and SVM_8) indicate the BL Lac-type ("bll") candidates identified by four different supervised machine-learning (SML) algorithms (Mclust Gaussian finite mixture models (M_8), decision trees (DT_8), random forests (RF_8), and SVMs (SVM_8)) with eight parameters in Kang et al. (2019a). Column 12 (LP17) lists the classifications ("bll" for BL Lac object, "unc" for uncertain, and "-" for a mismatched source by cross-comparison) in Lefaucheur & Pita (2017) using multivariate classifications. Column 13 (Chi16) reports the classifications in Chiaro et al. (2016) using ANN machine-learning techniques. Column 14 (Y17) shows the identified BL Lac objects reported in Yi et al. (2017) by researching the spectral index. Column 15 ($Class_O$) reports the optical classification (identified BL Lac object types based on optical spectroscopic) in Álvarez Crespo et al. (2016b) (a), Massaro et al. (2016) (b); Ajello et al. (2017) (c); Peña-Herazo et al. (2017) (d) Marchesi et al. (2018) (e); Desai et al. (2019) (f); Marchesini et al. (2019) (g); or/and The Fermi-LAT collaboration (2019) (h), respectively.

potential classification of BCUs, but the test error rate >0.11 (e.g., Paper I) is still very large. Due to the very large misclassified value, FSRQs and BL Lac objects may be misclassified. A more efficient (high-confidence) method for evaluating the potential classification of the BCUs may be necessary, and needs to be further addressed. On the other hand, in fact, in this work, our aim is to obtain a more precise conclusion with the least, most direct observation with the simplest method. Although there is still some artificiality in limiting the boundary value of "$a_i < X$ candidate zone", the result of "$a_i < X$ candidate zone" is stable. Here, only a part of BL Lac objects are classified from the BCUs, but not the

Table 4
The Comparison Results

Class (1)	N_X (2)	M_8 (3)	DT_8 (4)	RS_8 (5)	SVM_8 (6)	Chi16 (7)	LP17 (8)	Y17 (9)	M16 (10)	3FHL (11)	D19 (12)	M19 (13)	M18 (14)	P17 (15)	A16 (16)	4FGL (17)
–							2		96	36	118	109	110	108	105	4
bll	120	117	120	120	118	119	116	118	24	41	2	11	10	12	15	63
												74				
fsrq	0	3	0	0	2	1	0	2	0	0	0	0	0	0	0	1
unc							2			43						52

Note. Column 1 shows the classifications (– represents the number of mismatch by cross-comparison, "bll," "fsrq," and "unc" indicate BL Lac object, FSRQ, and uncertain type respectively). Column 2 is the number of sources (N_X) obtained by the $a_i < X$ candidate zone. The comparison results of Mclust Gaussian Mixture Modeling (M_8), decision tree (DT_8), RF (RS_8), and SVM (SVM_8) using eight parameters in Kang et al. (2019a) are listed in Columns 3–6, respectively. The results of cross-comparison with Chiaro et al. (2016, Chi16); Lefaucheur & Pita (2017, LP), and Yi et al. (2017, Y17) are shown in Columns 7–9, respectively. Columns 10–17 exhibit the results of cross-comparison with Massaro et al. (2016, M16); Ajello et al. (2017, 3FHL); Desai et al. (2019, D19); Marchesini et al. (2019, M19); Marchesi et al. (2018, M18); Peña-Herazo et al. (2017, P17); Álvarez Crespo et al. (2016b, A16) and The Fermi-LAT collaboration (2019, 4FGL), respectively, where 74 sources (also see Columns 18 in Table 3) are obtained from cross-matching these results (M16, 3FHL, D19, M19, M18, P17, A16, and 4FGL).

majority. The results likely provide some clues to the further study. For instance, it can contribute to subsequent source selections in the spectroscopic observation campaigns needed to confirm their real nature and, possibly, determine their redshifts (see, e.g., Ajello et al. 2014) and perform population studies of the remaining unassociated γ-ray sources (e.g., see Acero et al. 2013; D'Abrusco et al. 2019 for some discussions). The result of this work may provide more samples for studying the jet physics of the population of HSP BL Lac objects, or some clues for the planning of the main targets for rigorous analyses and multiwavelength observational campaigns (e.g., Chiaro et al. 2019). The empirical candidate zone gives higher confidence results with higher probabilities for $P_{\rm Bi}$ (see Table 4 in Paper I) that a BCU i belongs to BL Lac object (B) classes. This can provide the observer with guidance on the selection of the observation target within the limited observation resources (e.g., observation equipment, time). However, the empirical method may still cause misjudgments in identifying the potential (optical) classification of blazars. The optical spectroscopic observations remain the most efficient and accurate way to determine the real nature of these sources.

For the 120 predicted BL Lac object candidates using the "$a_i < X$ candidate zone" in the work, we also test the independence between the known classification 414 FSRQs using the two sample test. The distributions of $\Gamma_{\rm ph}$, VI, and $F_{\rm R}$ between the 414 FSRQs and the 120 identified BL Lac object candidate groups are significantly different. The two-sample Kolmogorov–Smirnov test gives $D = 0.725$, and the p-value $p_1 = 0$; the Welch Two Sample t-test gives $t = 38$, $df = 926$, and the p-value $p_2 < 1.0\text{E}{-6}$; while the Wilcoxon rank sum test with a continuity correction gives $W = 416{,}470$ and the p-value $p_3 < 1.0\text{E}{-6}$ for all three of the parameters (see Table 1). For other (one or two) parameter combinations, the test results are also reported in Table 1, which indicates that there is a strong separation between the 120 predicted BL Lac object candidates and the known classification of 414 FSRQs, which further verifies our results from another perspective.

We should note that, in Figure 1 (right column), if only two premises should be satisfied simultaneously, it would be that more sources can be selected as possible BL Lac candidates. For example, considering the lower, middle, and upper panels of Figure 1, there are an extra 57 BCUs with a misjudged rate (a probability that FSRQs are misclassified as BL Lac objects) $\eta = 10/414 \simeq 2.415\%$ (see Table 5) in the range ($\Gamma_{\rm ph} < 2.187$ and $\log F_{\rm R} < 2.258$) in the $\Gamma_{\rm ph} - \log F_{\rm R}$ panel (the lower panel of the right column in Figure 1). There are an extra 22 BCUs with a misjudged rate $\eta = 14/414 \simeq 3.382\%$ (see Table 5) in the range ($\Gamma_{\rm ph} < 2.187$ and $\log{\rm VI} < 1.702$) in the $\Gamma_{\rm ph} - \log$ VI panel (the middle panel of right column in Figure 1). There are an extra 55 BCUs (obtained easily from the the 3LAC website version) with a misjudged rate $\eta = 10/414 \simeq 2.415\%$ (see Table 5) in the range ($\log$ VI < 1.702 and $\log F_{\rm R} < 2.258$) in the $\log F_{\rm R} - \log$ VI panel (the upper panel of right column in Figure 1). These sources (57, 22, and 55) have a larger misjudged rate ($\eta > 2.4\%$); although we did not conclusively evaluate their potential classifications (FSRQs and BL Lac objects), it may be helpful for source selection in the spectroscopic observation campaigns in the future to further diagnose their optical classifications (see, e.g., Massaro et al. 2013; Yi et al. 2017 for the some discussions). In addition, if only one parameter is considered, a bigger misjudged error is introduced (see Table 5). Whether these three parameters ($\Gamma_{\rm ph}$, log VI, and $\log F_{\rm R}$) are the optimum combination of parameters needs to be further tested.

In addition, it must be highlighted that, in this work, the selection effects should be cautious (e.g., sample and method; see Kang et al. 2018, 2019a for the detail discussions), which may affect the source distributions and the results of the analysis. However, this work provides a simple direct method to distinguish the BL Lac objects from the BCUs based on the

Table 5
Source Numbers in Different Boundary Conditions

Parameters (1)	$\eta_{1\sigma}$ (2)	$N_{1\sigma}$ (3)
$\Gamma_{\rm ph}$, log VI, log$F_{\rm R}$	(3/414)	120
$\Gamma_{\rm ph}$, log $F_{\rm R}$	(10/414)	177
$\Gamma_{\rm ph}$, log VI	(14/414)	142
log VI, log $F_{\rm R}$	(10/414)	175
$\Gamma_{\rm ph}$	(66/414)	212
log $F_{\rm R}$	(65/414)	289
log VI	(48/414)	222

Note. Column 1 shows the parameters satisfied simultaneously. Column 2 is the misjudged rate ($\eta_{1\sigma}$) in the boundary value with a one-sided confidence interval for the 1σ confidence level. Column 3 is the number of BL Lac object candidates ($N_{1\sigma}$) selected from the BCUs in the boundary value with a one-sided confidence interval for the 1σ confidence level.

direct observational data. As the expansion of the sample, whether the proposed analysis ($a_i < X$ candidate zone) in this work is always robust and effective, that uses a large and complete sample (e.g., the upcoming 4LAC) is needed to further test and address the issue.

5. Summary

In this work, we proposed an analysis to evaluate the potential optical classification of BCUs. Based on the 3LAC Clean Sample, we collect 1418 Fermi blazars with three parameters of photon spectral index, variability index, and radio flux. We study the distributions of the FSRQs and BL Lac objects based on the scatterplots of these three parameters. We find that there are almost no FSRQs falling in a range $\Gamma_{\rm ph} < a_1$, $\log F_{\rm R} < a_2$ and $\log {\rm VI} < a_3$ for these three parameters. However, some BL Lac objects lie in the zone ($a_i < X$). Therefore, we suggest that it may be an invalid zone for FSRQs, but may be a candidate zone for BL Lacs (called "$a_i < X$ candidate zone" for BL Lacs). Using one-sample normal distribution tests for the $\Gamma_{\rm ph}$, VI, and $F_{\rm R}$ of the FSRQs, which show that these three variables have normal distributions. We assume that the lowest one-sided confidence interval values are treated as the boundary values a_i of these three parameters. In the unilateral 1σ confidence level, $a_1 = 2.187$, $a_2 = 2.258$, and $a_3 = 1.702$ are calculated. Assuming $\Gamma_{\rm ph} < 2.187$, $\log F_{\rm R} < 2.258$, and $\log {\rm VI} < 1.702$ are satisfied simultaneously, we apply the "$a_i < X$ candidate zone" to the BCUs, and then obtain 120 potential BL Lac object candidates. We compared the 120 potential BL Lac object candidates with some other recent (statistical) results, and find that almost all of the results are consistent with the results that have been identified as BL Lac objects in SML (or other statistical) methods. We also compared the 120 potential BL Lac object candidates with other spectroscopic certification results, and find most of the 120 (74) sources have been identified as BL Lac objects by spectroscopic observations (see Tables 4 and 5). Therefore, we suggest that the empirical candidates zone ($a_i < X$) may be a good criterion (high-confidence) for evaluating BL Lac object candidates only based on the direct observational data of $\Gamma_{\rm ph}$, VI, and $F_{\rm R}$. Although the proposed approach only identifies some of the BL Lac object candidates in the BCUs, not the majority. The results are stable and have a higher degree of confidence.

We thank the anonymous referee for very constructive and helpful comments and suggestions, which greatly helped us to improve our paper. This work is partially supported by the National Natural Science Foundation of China (grant Nos. 11763005, 11873043, 11847091, and U1931203), the Science and Technology Foundation of Guizhou Province (QKHJC[2019] 1290), the Research Foundation for Scientific Elitists of the Department of Education of Guizhou Province (QJHKYZ[2018] 068), the Open Fund of Guizhou Provincial Key Laboratory of Radio Astronomy and Data Processing (KF201811), the Science and Technology Platform and Talent Team Project of Science and Technology Department of Guizhou Province (QKH ∗ Platform & Talent[2018]5777, [2017]5721), and the Research Foundation of Liupanshui Normal University (LPSSYKJTD201901, LPSSY201401, LPSSYSSDPY201704, LPSZDZY2018-03, LPSSYZDXK201801, and LPSSYsyjxsfzx201801).

ORCID iDs

Shi-Ju Kang https://orcid.org/0000-0002-9071-5469
Qingwen Wu https://orcid.org/0000-0003-4773-4987
Bin-Bin Zhang https://orcid.org/0000-0003-4111-5958

References

Abdo, A. A., Ackermann, M., Agudo, I., et al. 2010, ApJ, 716, 30
Acero, F., Ackermann, M., Ajello, M., et al. 2015, ApJS, 218, 23
Acero, F., Donato, D., Ojha, R., et al. 2013, ApJ, 779, 133
Ackermann, M., Ajello, M., Atwood, W. B., et al. 2015, ApJ, 810, 14
Ajello, M., Atwood, W. B., Baldini, L., et al. 2017, ApJS, 232, 18
Ajello, M., Romani, R. W., Gasparrini, D., et al. 2014, ApJ, 780, 73
Álvarez Crespo, N., Masetti, N., Ricci, F., et al. 2016a, AJ, 151, 32
Álvarez Crespo, N., Massaro, F., D'Abrusco, R., et al. 2016b, Ap&SS, 361, 316
Álvarez Crespo, N., Massaro, F., Milisavljevic, D., et al. 2016c, AJ, 151, 95
Chiaro, G., Meyer, M., Di Mauro, M., et al. 2019, ApJ, 887, 104
Chiaro, G., Salvetti, D., La Mura, G., et al. 2016, MNRAS, 462, 3180
D'Abrusco, R., Álvarez Crespo, N., Massaro, F., et al. 2019, ApJS, 242, 4
Desai, A., Marchesi, S., Rajagopal, M., & Ajello, M. 2019, ApJS, 241, 5
Fan, J. H., Yang, J. H., Liu, Y., et al. 2016, ApJS, 226, 20
Hassan, T., Mirabal, N., Contreras, J. L., & Oya, I. 2013, MNRAS, 428, 220
Kang, S.-J., Fan, J.-H., Mao, W., et al. 2019a, ApJ, 872, 189
Kang, S.-J., Li, E., Ou, W., et al. 2019b, ApJ, 887, 134
Kang, S.-J., Wu, Q., Zheng, Y.-G., et al. 2018, RAA, 18, 056
Kaur, A., Ajello, M., Marchesi, S., & Omodei, N. 2019, ApJ, 871, 94
Klindt, L., van Soelen, B., Meintjes, P. J., & Väisänen, P. 2017, MNRAS, 467, 2537
Landoni, M., Massaro, F., Paggi, A., et al. 2015, AJ, 149, 163
Landoni, M., Paiano, S., Falomo, R., Scarpa, R., & Treves, A. 2018, ApJ, 861, 130
Laurent-Muehleisen, S. A., Kollgaard, R. I., Feigelson, E. D., Brinkmann, W., & Siebert, J. 1999, ApJ, 525, 127
Lefaucheur, J., & Pita, S. 2017, A&A, 602, A86
Marchesi, S., Kaur, A., & Ajello, M. 2018, AJ, 156, 212
Marchesini, E. J., Masetti, N., Chavushyan, V., et al. 2016, A&A, 596, A10
Marchesini, E. J., Peña-Herazo, H. A., Álvarez Crespo, N., et al. 2019, Ap&SS, 364, 5
Massaro, E., Giommi, P., Leto, C., et al. 2009, A&A, 495, 691
Massaro, F., Álvarez Crespo, N., D'Abrusco, R., et al. 2016, Ap&SS, 361, 337
Massaro, F., D'Abrusco, R., Landoni, M., et al. 2015, ApJS, 217, 2
Massaro, F., D'Abrusco, R., Tosti, G., et al. 2012, ApJ, 750, 138
Massaro, F., Masetti, N., D'Abrusco, R., Paggi, A., & Funk, S. 2014, AJ, 148, 66
Massaro, F., Paggi, A., Errando, M., et al. 2013, ApJS, 207, 16
Paiano, S., Falomo, R., Franceschini, A., Treves, A., & Scarpa, R. 2017a, ApJ, 851, 135
Paiano, S., Falomo, R., Landoni, M., Treves, A., & Scarpa, R. 2017b, FrASS, 4, 45
Peña-Herazo, H. A., Marchesini, E. J., Álvarez Crespo, N., et al. 2017, Ap&SS, 362, 228
Peña-Herazo, H. A., Massaro, F., Chavushyan, V., et al. 2019, Ap&SS, 364, 85
R Core Team 2019, R: A Language and Environment for Statistical Computing (Vienna: R Foundation for Statistical Computing), https://www.R-project.org/
Ricci, F., Massaro, F., Landoni, M., et al. 2015, AJ, 149, 160
Salvetti, D., Chiaro, G., La Mura, G., & Thompson, D. J. 2017, MNRAS, 470, 1291
Shaw, M. S., Romani, R. W., Cotter, G., et al. 2013, ApJ, 764, 135
Singal, J. 2015, MNRAS, 454, 115
Singal, J., Petrosian, V., & Ajello, M. 2012, ApJ, 753, 45
Stickel, M., Padovani, P., Urry, C. M., Fried, J. W., & Kuehr, H. 1991, ApJ, 374, 431
Stocke, J. T., Morris, S. L., Gioia, I. M., et al. 1991, ApJS, 76, 813
The Fermi-LAT collaboration 2019, arXiv:1902.10045
Urry, C. M., & Padovani, P. 1995, PASP, 107, 803
Yi, T.-F., Zhang, J., Lu, R.-J., Huang, R., & Liang, E.-W. 2017, ApJ, 838, 34
Zhu, K., Kang, S.-J., & Zheng, Y.-G. 2020, arXiv:2001.06010